Integration of Microfluidics With a Love Wave Sensor for the Fabrication of a Multisample Analytical Microdevice

Konstantinos Mitsakakis, Angeliki Tserepi, and Electra Gizeli, *Member, IEEE*

***Abstract*—A novel approach for multisensing has been developed based on the integration of a parallel-channel microfluidic module with a surface acoustic wave (SAW) sensor chip. The microfluidic module was used to compartmentalize the surface of a single SAW sensor into N equal subareas in order to deliver and detect multiple samples on the sensor. The design concerns and fabrication procedure using soft lithography of polydimethylsiloxane are described. Successful demonstration of a four-channel module is reported, along with a sensitivity evaluation and comparison with a standard flow cell used so far. Very promising results were revealed during the tests concerning the system's operation with liquid samples. The reliability and reproducibility of the results in all four subareas render the proposed setup very suitable for biological testing and screening of various biomolecules in an array format. [2008-0031]**

***Index Terms*—Microfluidics, polydimethylsiloxane (PDMS), soft lithography, surface acoustic waves (SAWs).**

I. Introduction

SURFACE acoustic wave (SAW) sensors as analytical microdevices have extensively been implemented in a wide range of applications. They have been used in vacuum chamber processes [1], as gas sensors for toxic agents [2], as biosensors operating in liquid for probing interactions and structural characteristics of various biomolecules at surfaces [3], [4], etc. They have also been used for measuring physical properties such as pressure changes [5], viscosity of liquids [6], and mechanical properties (shear moduli) of elastic and viscoelastic films [7].

The vast majority of the above applications focus on testing one sample per sensor. However, in applications like toxic gas sensing, chemical testing, identification of pollutants, biosensing, drug screening, etc., there is an ever-increasing demand for multianalyte detection and analysis [8]. SAW sensors application to multisensing has been very limited in gas-phase sensing [9]–[12]. Few efforts have been directed toward the development of SAW array biosensors [13], [14]. The main idea has been the placement of several SAW delay lines one next to the other to fabricate a linear array. This approach, however, requires high-complexity electronics for the real-time data acquisition. Moreover, it lacks versatility since the number of samples that the user is allowed to probe is strictly limited by the number of sensor elements incorporated in the array.

To overcome these issues, a new concept is proposed for SAW multisensing, based on microfluidics. Microfluidic structures have rapidly entered into the microanalytical world due to some major advantages they possess; the reduction of dead volume, the low sample consumption, the fast analysis times, the ability for parallelization, and for performing various integrated functions (dispensing, separation, mixing, delivery of liquids, etc.) are some of the features that have promoted microfluidic devices in numerous applications such as biosensing, microarrays, micrototal analysis systems, and lab-on-chips within a timeframe of approximately 15 years [15]–[18].

The idea of this paper is to integrate microfluidics with the SAW sensor device toward the development of a multisample sensing setup. In particular, instead of placing N sensors in a line to form an array, it is proposed to divide the surface of a single sensor into N subareas using an N-parallel-channel microfluidic module, achieving, thus, a "multisample-per-sensor" configuration. An important advantage of this novel arrangement is that complex electronics are avoided since the measurement platform is the same as the one used for a single SAW device. In addition, the fabrication of the modules is low cost and time saving, as well as versatile, since it is feasible to make as many microchannels as the application demands.

This paper reports on the design considerations and the fabrication steps of the microfluidic module taking in mind the specific characteristics of the SAW sensor. Subsequently, the testing and evaluation of the proposed "microfluidics-on-SAW" (μF-on-SAW) system in terms of its functionality, sensitivity, and reliability are presented and compared to the standard SAW setup used so far.

II. Sensor Platform: Love Wave Devices

A. Operation Principle

The piezoelectric sensor's principle of operation is, essentially, the interaction of a SAW with matter. The material under test can be a rigid mass layer [19], a purely viscous liquid [20],

Manuscript received February 11, 2008; revised April 22, 2008. First published July 18, 2008; last published August 1, 2008 (projected). The work of K. Mitsakakis was supported by the Public Welfare Foundation "Propondis." Subject Editor A. Ricco.

K. Mitsakakis is with the Institute of Molecular Biology and Biotechnology, Foundation for Research and Technology Hellas, 711 10 Heraklion, Greece, and also with the Department of Materials Science and Technology, University of Crete, 71 409 Heraklion, Greece (e-mail: kmits@imbb.forth.gr).

A. Tserepi is with the Institute of Microelectronics, National Center for Scientific Research "Demokritos," 153 10 Athens, Greece (e-mail: atserepi@imel.demokritos.gr).

E. Gizeli is with the Institute of Molecular Biology and Biotechnology, Foundation for Research and Technology Hellas, 711 10 Heraklion, Greece, and also with the Department of Biology, University of Crete, 71 409 Heraklion, Greece (e-mail: gizeli@imbb.forth.gr).

Digital Object Identifier 10.1109/JMEMS.2008.927173

1057-7157/$25.00 © 2008 IEEE

Authorized licensed use limited to: WARWICK UNIVERSITY. Downloaded on January 18, 2010 at 14:32 from IEEE Xplore. Restrictions apply.

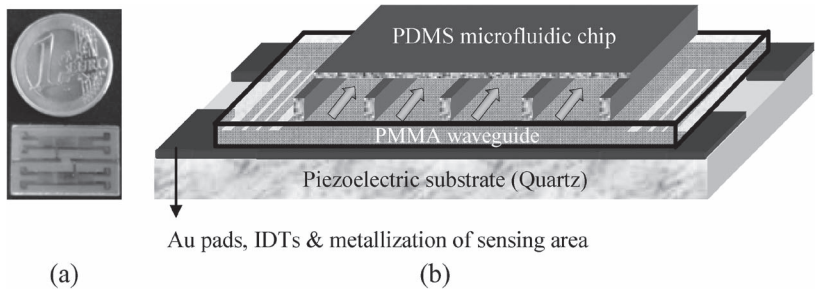

Fig. 1. (a) Dual SAW sensor chip. (b) Three-dimensional representation of a μF-on-SAW setup.

a viscoelastic film [21], as well as combinations of the above (multilayer structures) [22]. In this paper and for the purpose of evaluation of the proposed μF-on-SAW setup, we focus on the viscous loading as a means of testing the system's sensitivity and performance. For liquid applications, the utilization of Rayleigh SAW is not suitable because of its surface-normal component of particle displacement, which imposes severe damping of the wave in liquid. Therefore, the shear-horizontal polarization is chosen. Shear-horizontal surface acoustic wave (SH-SAW) is an acoustic evanescent wave and exponentially decays toward the propagation-normal direction as it propagates within the medium. Therefore, a penetration depth δ is defined as the effective length along which the amplitude of particle displacement decays over the 1/e of its surface value. It is a function of the fluid density ρ and viscosity η as well as the sensor operating angular frequency ω [20]

$$\delta = \sqrt{\frac{2\eta}{\rho\omega}}. \tag{1}$$

The sensor is sensitive only to events taking place within the volume defined by the penetration depth. For the sensor that was used with center frequency at 155 MHz, δ is approximately 50 nm in water environment. Regarding the sensitivity of an SH-SAW sensor, it is predominantly a function of its operating frequency [23]; the higher the frequency, the higher the sensitivity. In order to enhance the sensor sensitivity, a thin polymer layer is spin coated on the piezoelectric substrate. This layer acts as a waveguide, supports the acoustic wave, and confines the acoustic energy in the vicinity of the sensor surface, rendering it more sensitive to surface perturbations. This configuration is known as the Love wave sensor [24].

The acoustic wave generated in the piezoelectric substrate of the sensor is a propagating plane wave. The complex wave propagation factor is related to its attenuation and velocity. These quantities are directly proportional to the amplitude and phase of the wave, respectively. The relationship between these wave characteristics and the liquid properties (density ρ and viscosity η) is summarized in the following two equations, where ΔA and $\Delta\varphi$ represent the change in wave amplitude and phase, respectively, and ω is the device operating angular frequency

$$\Delta \mathrm{A} = c_1\sqrt{\frac{\omega\rho\eta}{2}} \tag{2}$$

$$\Delta\varphi = c_2\sqrt{\frac{\omega\rho\eta}{2}}. \tag{3}$$

The proportionality constants c_1, c_2 depend on the device material and geometry, the surface particle velocity, and the SAW power density. All these sensor-related parameters are incorporated in the constants and, as long as the device used is the same, the values for c_1, c_2 remain constant. Therefore, according to (2) and (3), both wave propagation parameters are proportional to the square root of density–viscosity product [6], [20], [25], and [26].

B. Sensor Chip Architecture and Measurement Instrumentation

The sensor chip we used is based on a 0.5-mm-thick Y-cut quartz crystal. Two sets of 100-nm-thick Au interdigital transducers (IDTs) were photolithographically patterned on top of quartz, while a 20-nm-thick Cr thin film was used as adhesive layer between quartz and Au. The IDTs have a split finger design with a period of 32 μm. Each chip consists of two sensors [Fig. 1(a)]. The waveguide material was polymethylmethacrylate (PMMA). An 8% (w/w) solution, prepared in 2-ethoxyethyl acetate 99+% (Aldrich), was spin coated on the device chip at 4000 r/min for 60 s using a P6700 series commercial spin coater (Specialty Coating Systems). A 3-D representation of a SAW sensor is shown in Fig. 1(b).

An HP 8753ES Network Analyzer (NA) was used in order to perform the measurements of ΔA and $\Delta\varphi$, along with an HPVEE software for data acquisition. The time-gating option of the NA was used in order to minimize undesired interference with electromagnetic feed-through and triple-transit signals. In addition, the NA was connected to a switch control unit (Agilent 3499A) so that both sensors could be simultaneously probed. The experimental setup is shown in Fig. 2.

The sensitivity S of the SAW sensor to viscous loading is expressed as the change in acoustic signal (either amplitude or phase) with respect to the change of $(\rho\eta)^{1/2}$. In other words,

$$S = \frac{d(\Delta\mathrm{Signal})}{d(\sqrt{\rho\eta})}. \tag{4}$$

In practice, the sensitivity is extracted by the slope of a ΔSignal versus $(\rho\eta)^{1/2}$ graph. This relationship remains linear up to a critical viscosity value, until which the sample is considered a Newtonian fluid. Beyond that, the signal reaches a saturation, and the sensor response can be explained by considering the liquid as Maxwellian and modeling it accordingly [27]. In this paper, the viscosity values of all samples lie within the linear region.

Authorized licensed use limited to: WARWICK UNIVERSITY. Downloaded on January 18, 2010 at 14:32 from IEEE Xplore. Restrictions apply.

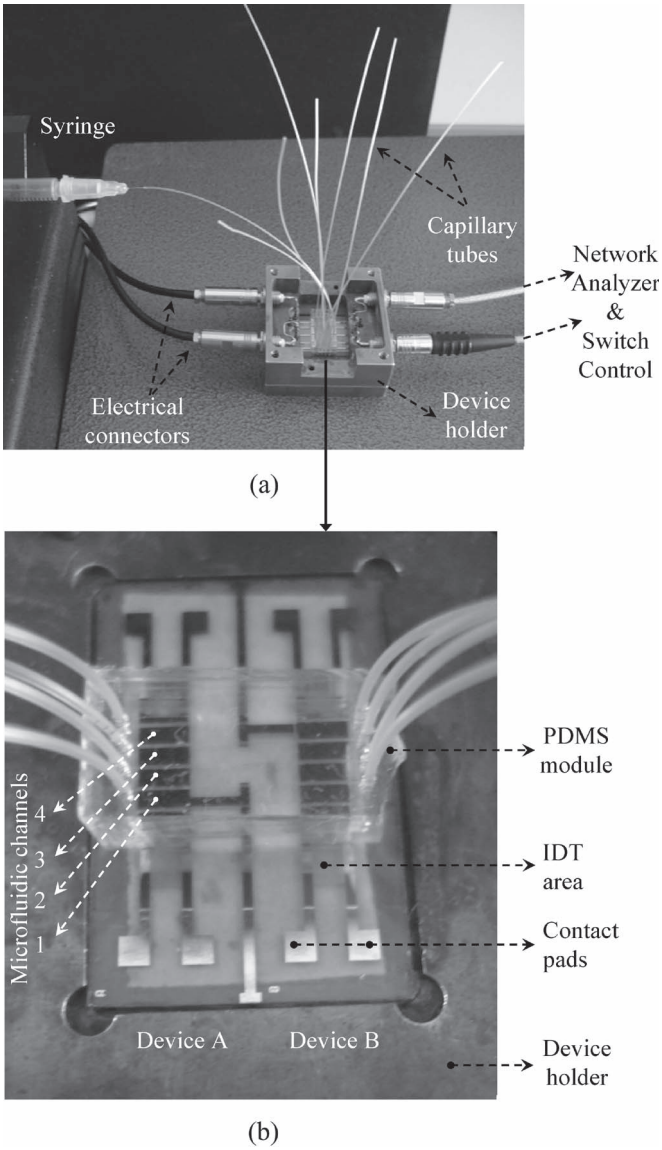

Fig. 2. (a) Experimental setup. (b) Close-up image of the sensor chip with the attached microfluidic module.

III. Design and Fabrication of the Microfluidic Modules

A. Microfluidic Module Design

The microfluidic module is intended to facilitate the separation of the SAW surface into subareas in order for multisample sensing to be achieved. That is why the design of the module suggests a parallel configuration of microchannels. Figs. 2(b) and 3(a) show the microfluidic module mounted on top of the SAW chip. For comparison reasons, Fig. 3(b) shows the setup with the standard flow cell made of plexiglass with two rectangular rubber gaskets for gentle contact with the sensor, and the device holder used for measurements over the total sensor surface.

The first issue of the design was the orientation of the microchannels, since two possible configurations were available: the microchannels' axis being: 1) parallel or 2) perpendicular to the direction of wave propagation (the k-vector). In the first case, the wavefront would overlap N different samples at any specific timeframe (N being the number of microchannels). The wavefront would, thus, undergo different time delay during its interaction with the different samples and break into partial wavefronts (Fig. 4). Eventually, the receiver IDTs would sense an interference signal between the N parts of the wavefront. This effect was experimentally verified by poor quality results and lack of reproducibility of signal change upon sample loading (data not shown). Such irregularities do not hold for the case of the perpendicular-to-k-vector orientation of the microchannels, which is why this design was selected, instead.

Having selected the microchannel orientation, the next step involved the design of microchannels' dimensions. These were selected considering two key factors: 1) the contact area between the sensor and the module and 2) the active area per microchannel. To elaborate, each microchannel is separated by its neighboring one by a polydimethylsiloxane (PDMS) "wall," which should be thick enough to facilitate good contact of the walls with the sensor surface and prevent leakage. Fig. 5(a) shows a "leaking" microchannel and Fig. 5(b) a functional module. On the other hand, a major concern that had to be taken into consideration was the piezoelectric nature of the SAW sensor; excessive contact area between the sensor and the module led to high damping of the wave and/or malfunction of the device due to signal distortion. Therefore, to compensate the pros and cons of the thickness of PDMS walls, the values were chosen for the wall thickness to be around 100–120 μm. The height of the microchannels was 100 μm, as defined by the fabrication procedure (Section III-B). With these dimensions, the active sample volumes are drastically minimized; volumes of 150–250 nL correspond to each sensing subarea, in contrast to typically 3.5 μL that correspond to the total sensing area of the standard flow cell. Finally, speaking of channel dimensions, it should be noted that for both water and glycerol samples used in the experiments the swelling ratio of PDMS was one [28], which indicates no swelling behavior of the material and, thus, no change in dimension or its properties upon its contact with the particular samples.

Another special feature of the design derives from the liquid state of the samples; the operation of the IDT electrodes is incompatible with liquid. Therefore, it is imperative that the IDT areas should be kept out of contact with the fluid under test, otherwise severe distortion of the wave properties would be caused. One option would be to simply let the module cover the IDT sets. This, however, would impose pressure on the IDT region and would, again, cause severe damping and distortion of the output signal. For this reason, the design includes a hollow "safety shell" located above the IDT sets in order to prevent their contact with both the liquid and the bulk material of the module.

Regarding the sample input and output, although the results presented in this paper derive only from one of the two sensors of the dual SAW chip, the length of the microchannels was designed big enough to allow liquid flow above both sensors of the chip. Therefore, this value was fixed at 12.75 mm, allowing the input and output of the liquid to take place outside the sensing areas to avoid any possible effect on the signal response. The edges of the microchannels (liquid input and

Authorized licensed use limited to: WARWICK UNIVERSITY. Downloaded on January 18, 2010 at 14:32 from IEEE Xplore. Restrictions apply.

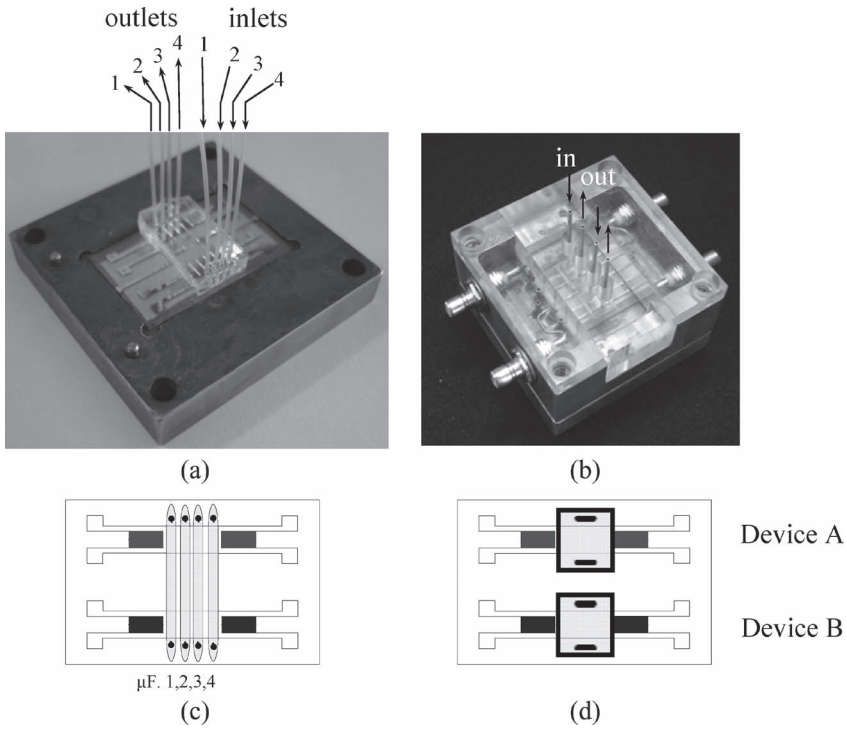

Fig. 3. (a) and (c) PDMS multichannel module with attached capillary tubes; image and top view sketch, respectively. The black circles in (c) represent the inlets and outlets of the microtubes right above the sensor. (b) and (d) Standard flow cell image and top-view sketch, respectively. The two bold rectangles in (d) indicate the two rubber gaskets, and the four bold ovals represent the inlets and outlets of the standard flow cell.

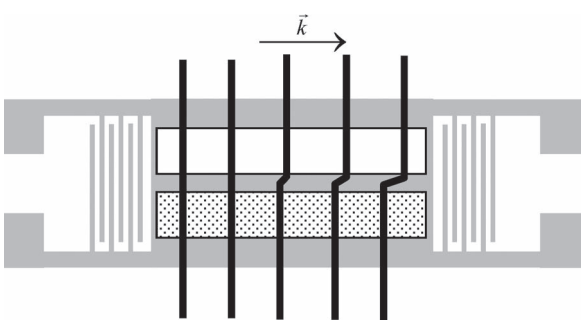

Fig. 4. (Black lines) Wavefronts traveling perpendicularly to the subareas orientation causing a different time delay. White and dotted regions represent two subareas with different samples.

output regions) were designed curved instead of rectangular to avoid bubble formation and sample remnants at these regions as well as incomplete wash-off, which could be possible in the case of rectangular-edged microchannels.

Taking into consideration the above design parameters and special features of the SAW sensor chip, the optimum dimensions of channel width and PDMS-wall thickness for the cases of three-, four-, and five-channel modules are summarized in Table I.

B. Fabrication Process of Microfluidics–Mold Fabrication

The microfluidic module was fabricated by means of soft lithography. This includes a group of procedures, which allows fast, cost-effective, and simple fabrication of microfluidic devices. Rapid prototyping is one major step, during which a master prototype is designed and fabricated with standard photolithographic techniques, and can be used over and over again as a mold. In the subsequent step of replica molding, PDMS, the material used in this application to make the micromodule,

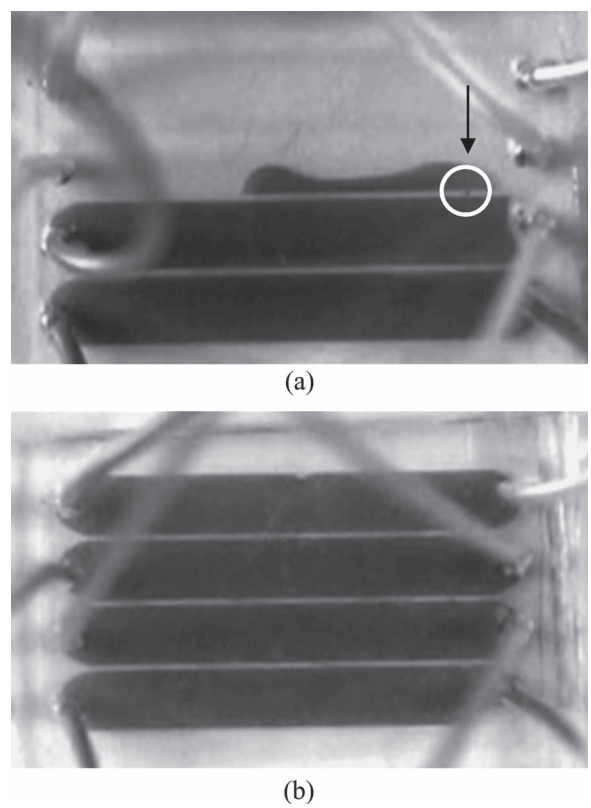

Fig. 5. (a) Leakage between two microchannels due to localized failure in contact. (b) Flow through intact microchannels.

Authorized licensed use limited to: WARWICK UNIVERSITY. Downloaded on January 18, 2010 at 14:32 from IEEE Xplore. Restrictions apply.

TABLE I
TYPICAL DIMENSIONS FOR THREE TYPES OF MICROFLUIDIC MODULES

Number of Channels	Channel Height (μm)	Channel Width (μm)	PDMS Wall Thickness (μm)	Sub-Area (mm^2)	Microchannel Volume (μl)	
					Total	Above each Sub-Area
3	100	1550	120	2.48	1.97	0.248
4	100	1100	120	1.76	1.40	0.176
5	100	900	110	1.44	1.14	0.144

is cast on the mold, and after specific thermal treatment, it acquires the negative pattern of the mold [29]–[31]. In this section, the procedure that was followed toward the fabrication of the microfluidic modules is presented in detail.

The design was made with AutoCAD and printed on a transparency with a high-resolution (2400 dpi) commercial printer. The transparency was used as an initial mask for patterning a 500-nm-thick Al-coated piece of glass (Al was deposited by thermal evaporation). This was done by means of negative photolithography of AZ(5214E) photoresist and subsequent wet etching of the Al with a mixture of H_3PO_4 and isopropyl alcohol 1 : 1. In this way, the patterns were directly transferred from the transparency to the Al mask, which was then used for all the subsequent photolithography processes.

The negative epoxy-type photoresist SU8 100 from MicroChem Corporation was used for the mold fabrication. The processing of SU8 included the following steps, according to the supplier's instructions: substrate pretreatment followed by spin-coating of SU8 on the Si substrate (Karl Suss RC8 spinner), and soft baking in order to form a 100-μm-thick SU8 layer. This thickness defines the depth of the microchannels. Exposure to i-line UV was done with a Karl Suss MJB3 mask aligner; various exposure times were examined for optimum crosslinking. Two kinds of filters were used; a narrow bandpass filter with a full-width at half-maximum of 55 nm in combination with a steplike filter that cuts off wavelengths below 365 nm, where SU8 presents too high absorbance and could result in too high exposure of the top part of the structures and, therefore, highly nonvertical walls [32]. The final processing steps included postexposure bake and development which took place in propylene glycol methyl ether acetate.

Upon completion of the processing, the structures were examined under an optical microscope in order to validate the efficiency of the procedure and the accuracy of the structures; very little profile of the SU8 walls was observed, i.e., deviation from the ideal vertical shape. This was of the order of 10% maximum, which does not affect the purposes of the current work.

C. Fabrication Process of Microfluidics–PDMS Processing and Replica Molding

Preparation of the PDMS involved mixing of the base resin with the curing agent Sylgard 184, supplied from Dow Corning Corporation, in a 10 : 1 ratio and degassing. After complete removal of the bubbles, the prepolymer mixture was cast on the SU8 mold, which was located in a 4.5-mm-deep metal holder. Last step was the thermal curing of PDMS and peeling off the thermally cross-linked PDMS from the SU8 mold. The elastomer modules were 4 mm thick, adjusted by the depth of the metal holder. The PDMS modules were diced from the "elastomer wafer" with a razor edge and precisely drilled with a bench drill machine (TBM 220) to open 0.5-mm-diameter vias and attach capillary microtubes made of low-density polyethylene (Scientific Commodities, Inc.) for fluid inlet and outlet. The microtubes were manually fixed on their correspondent drilled positions on the PDMS module. The lack of glue or any other adhesive means is a great advantage because: 1) it eliminates the module contamination and 2) it allows the replacement of one or more microtubes at any moment without having to dispose of the PDMS module. Fig. 6 shows the (a) cross-sectional and (b) top view of scanning-electron-microscopy images of three-, four-, and five-channel PDMS microfluidic modules. It clearly appears that the end-to-end

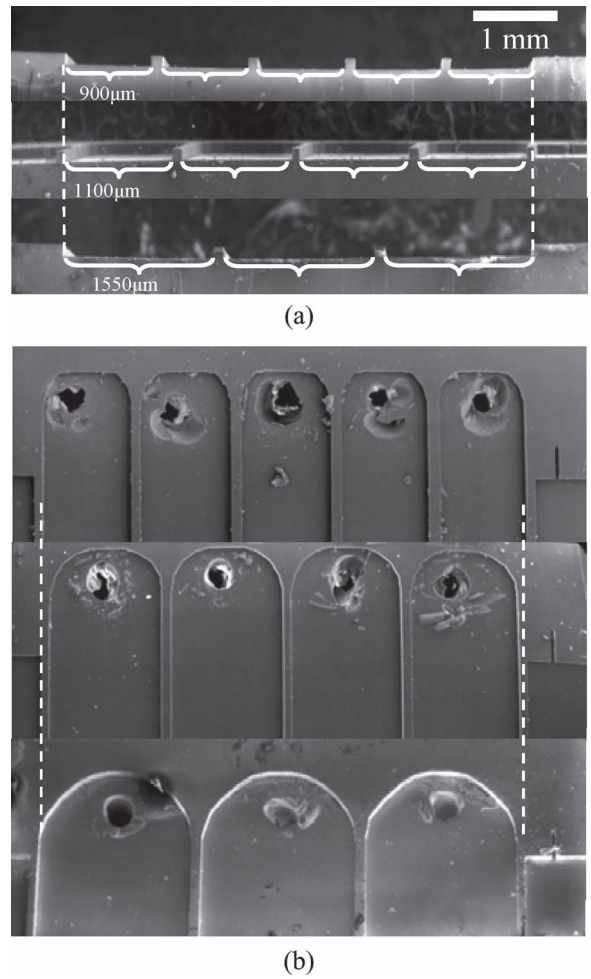

Fig. 6. Scanning electron microscope images of three-, four-, and five-channel microfluidic modules. (a) Cross-sectional view. (b) Top view. All images were taken with 20x magnification.

Authorized licensed use limited to: WARWICK UNIVERSITY. Downloaded on January 18, 2010 at 14:32 from IEEE Xplore. Restrictions apply.

TABLE II
FEATURES OF GLYCEROL SAMPLES USED IN THE EXPERIMENTS

Sample Serial No	Glycerol Concentration (w/w)	Square Root of Density-Viscosity Product ($kg \cdot m^{-2} \cdot s^{-1/2}$)
gly#1	15.37%	1.41
gly#2	25.63%	1.55
gly#3	32.87%	1.74
gly#4	37.34%	1.92
gly#5	42.29%	2.05
gly#6	46.72%	2.20

width is the same for all chips, as they are all intended to fit in the same sensing area of the SAW sensor. The difference in the microchannels width is noticeable, as well as part of the "safety shell" at both sides of the microchannels for the IDTs protection [Fig. 6(b)].

To ensure the reusability of the PDMS modules and the uniform regeneration of the sensor surface after each experiment, the modules were reversibly bound to the sensor surface. Specifically, the PDMS modules formed reversible sealing on the sensor when pressed against the latter; a slight pressure was enough to seal the module on the sensor. This reversible sealing is possible because PDMS is flexible and can conform to minor imperfections in a "flat" surface making van der Waals contact with this surface. This method of sealing is water tight and fast and occurs at room temperature. Simply peeling the PDMS off the flat surface breaks this reversible seal [30]. However, to ensure the stability of the module, a plastic cover with properly designed holes in order not to obstruct the microtubes was screwed on top of the PDMS module in order to apply gentle external pressure on the latter.

IV. CHARACTERIZATION OF THE μF-ON-SAW SETUP

For the qualitative and quantitative evaluation of the performance of the microfluidic module upon its integration with the SAW sensor chip, aqueous glycerol solutions were used in concentrations varying from 15%–50% (w/w). Glycerol has widely been used for the calibration and evaluation of performance of SAW sensor setups [6], [25], [27]. In addition, assuming that the surface roughness of the PMMA is negligible and based on the fact that glycerol has not been observed to bind to the PMMA surface, it can be safely considered that glycerol presents a purely viscous behavior when it is applied on the sensor.

The viscosity of glycerol solutions was experimentally measured, using a concentric-cylinder-geometry Anton Par viscometer, at 25 °C and at 264 min^{-1} shear rate. The glycerol solutions were considered Newtonian; this was also experimentally verified since the viscosity remained constant for various shear rates. Table II summarizes the values for the concentration and the square root of density–viscosity product of the glycerol solutions.

Initial experiments were carried out using the standard flow cell covering the total SAW surface, in order to acquire the sensitivity profile over the total sens ing area for viscous loading and have a basis of comparison for the subsequent evaluation of the microfluidic module. The sensing area exposed to the standard flow cell is 7.44 mm^2. The subareas as defined by the microchannels are listed in Table I. In order to be able to combine results from both standard flow cell and microfluidics, the acoustic signal change was normalized to surface area. The flow rate in all cases was 10 μL/min, achieved with a HARVARD PHD 2000 programmable syringe pump.

Regarding the total sensing area, the output signal acquired at the receiver IDTs is essentially an average of the "events" taking place across the surface. In the case of the microchannels, as the total surface is discretely divided into subareas, the output acoustic signal is the sum of the events taking place in all subareas. Therefore, during the injection of a sample through microchannel #i, there is no sample in the rest of microchannels in order to avoid convolution and undesirable contributions (see Table III for sequence of sample injections). Instead, water remains in the unused microchannels in a "static" way, i.e., without flow. Although this could imply longer duration of the experiment, in reality, this was not the case as it was proved by initial tests for time tradeoff between the standard and the μF-on-SAW setups. It was estimated that for a typical experiment of four glycerol samples using the standard flow cell the elapsed time was around 2000 s. Equivalently, the time for sequentially running one sample per microchannel (i.e., total of four samples) was, again, approximately 2000 s (including rinsing). To conclude, the fact that the μF-on-SAW does not lag in experimental time (compared to sequential standard flow cell use) in combination with the miniaturized sample volumes (Section III-A) and the optimized reproducibility of measurements render the μF-on-SAW a powerful tool for multisample analysis.

To ensure that the existence of nonflowing water in the rest of microchannels—other than the one in use—does not affect the acquired signal, water was injected and left in the microchannels for a sufficient duration of time; no change in the baseline of the signal was observed.

Fig. 7 shows the real-time response of the SAW sensor in terms of the amplitude of the acoustic wave, when the four-channel microfluidic module was used; a similar response was observed for the phase of the acoustic wave. Each group of six signal changes corresponds to successive injections of the six glycerol solutions through microchannels #1, 2, 3, and 4. Following the injection of each sample, the signal drops accordingly and, on rinsing, returns at its initial baseline, which ensures that glycerol does not adsorb on PMMA, nor that there are any mass loading effects due to surface roughness-induced liquid trapping. A very small signal drift or deviation from complete return of the baseline is due to temperature fluctuations and/or other environmental reasons. This drift, though, is not relevant to the use of the microfluidic module, since it is also observed in experiments using the standard flow cell (data not shown).

A crucial condition for the viability and reliable functionality of the μF-on-SAW system is that, upon loading the same sample on the various subareas, the sensor response should be the same or, at least, consistently different (so that some sort of calibration can be done according to the spatial location of each microchannel). In order to test this, the change of acoustic signal was extracted from the real-time data and was plotted for each sample and for each of the four microchannels (Fig. 8).

Authorized licensed use limited to: WARWICK UNIVERSITY. Downloaded on January 18, 2010 at 14:32 from IEEE Xplore. Restrictions apply.

TABLE III
CONTENT OF EACH MICROFLUIDIC CHANNEL DURING THE EXPERIMENT

μF channel #1	μF channel #2	μF channel #3	μF channel #4
	Water for equilibrium in all microchannels		
gly#6	"static" water	"static" water	"static" water
rinse	"static" water	"static" water	"static" water
gly#5	"static" water	"static" water	"static" water
rinse	"static" water	"static" water	"static" water
rest of samples & rinse	"static" water	"static" water	"static" water
"static" water	gly#6	"static" water	"static" water
"static" water	rinse	"static" water	"static" water
"static" water	gly#5	"static" water	"static" water
"static" water	rinse	"static" water	"static" water
"static" water	rest of samples & rinse	"static" water	"static" water
"static" water	"static" water	gly#6	"static" water
"static" water	"static" water	gly#5	"static" water
"static" water	"static" water	rinse	"static" water
"static" water	"static" water	rest of samples & rinse	"static" water
"static" water	"static" water	"static" water	gly#6
"static" water	"static" water	"static" water	rinse
"static" water	"static" water	"static" water	gly#5
"static" water	"static" water	"static" water	rinse
"static" water	"static" water	"static" water	rest of samples & rinse
	End of experiment		

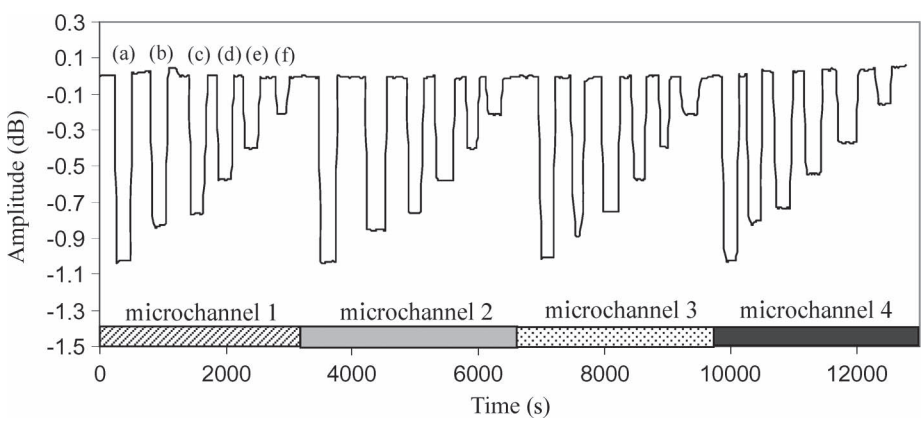

Fig. 7. Real-time representation of the acoustic wave amplitude. Series of injections was as follows: (a) Gly#6. (b) Gly#5. (c) Gly#4. (d) Gly#3. (e) Gly#2. (f) Gly#1. The same sequence continues for the rest of the microchannels. The serial number of the samples corresponds to specific concentration, as it appears in Table II.

Each group of bars indicates the surface-normalized signal change upon loading of a specific sample in the four different microchannels.

Interestingly, it was observed that when the same sample (e.g., gly#1) was injected in different microchannels, i.e., it flowed over different locations on the sensor surface, the signal response obtained was essentially the same. The maximum observed deviation was 6% for amplitude and 8% for phase change, as estimated by the ratio of the maximum and minimum values of signal change. This suggests that the sensor response is independent of the subarea location. The above applies to the whole range of glycerol concentrations that were tested, with maximum deviations for the rest of glycerol solutions of the order of only 5% and 6%–8% for amplitude and phase changes, respectively. Finally, the last bar of each group represents the surface-normalized signal change when the standard flow cell was used on the total surface. As it appears, there is a satisfactory agreement between the two setups (upon surface normalization of the signal), with very few exceptions of deviation up to 10%, which, however, is considered to be within the experimental error.

The sensitivity of the SAW system upon viscous loading is evaluated through the surface-normalized change of the acoustic signal with respect to the sample's $(\rho\eta)^{1/2}$ (4). The relationship of these quantities is linear for the total area and for the viscosities range that was used (2) and (3). Fig. 9 summarizes the ΔSignal/area versus $(\rho\eta)^{1/2}$ plots for all microchannels and the standard flow cell. It is noticeable that, for

Authorized licensed use limited to: WARWICK UNIVERSITY. Downloaded on January 18, 2010 at 14:32 from IEEE Xplore. Restrictions apply.

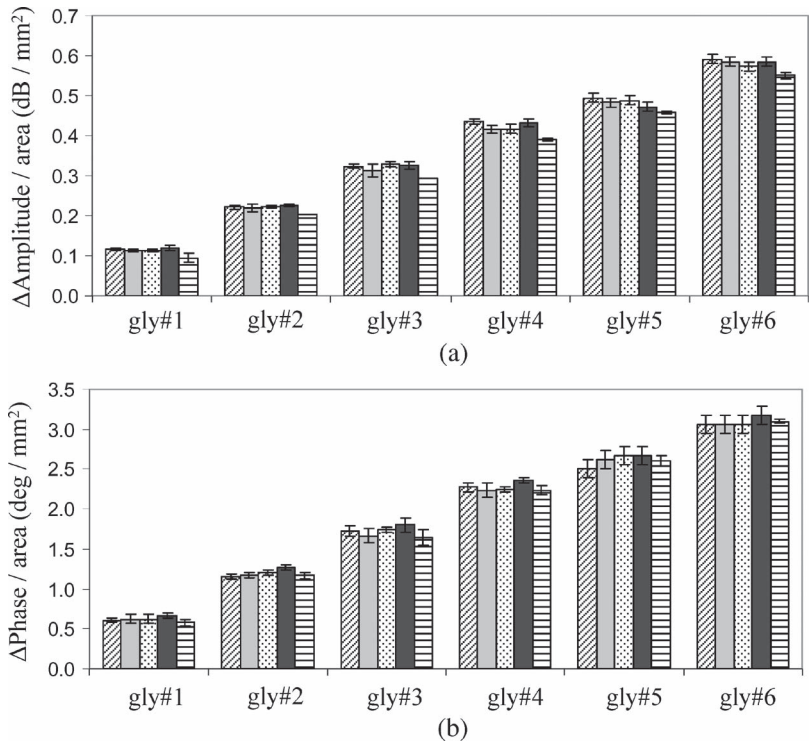

Fig. 8. Surface-normalized change in acoustic signal for each sample and in each microchannel. (a) Amplitude change. (b) Phase change. "μF" in index stands for "microfluidic channel."

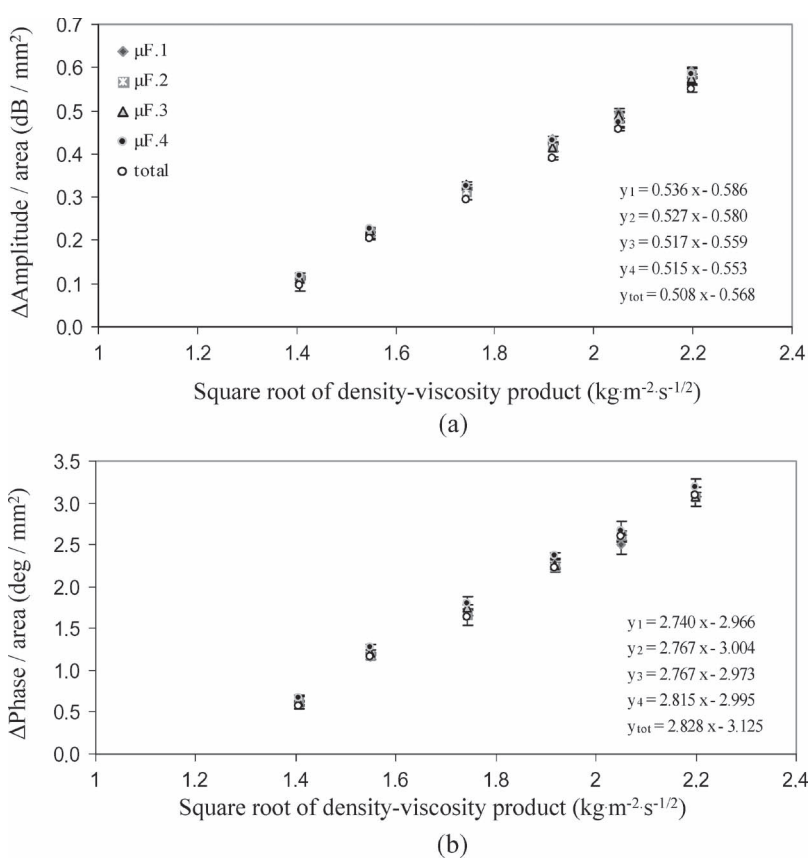

Fig. 9. Signal change as a function of the square root of density–viscosity product. (a) Amplitude change. (b) Phase change. The equations refer to the linear trendlines. The slopes represent the sensitivities of the four subareas and the total area.

Authorized licensed use limited to: WARWICK UNIVERSITY. Downloaded on January 18, 2010 at 14:32 from IEEE Xplore. Restrictions apply.

the examined viscosities, the linearity between ΔA (and $\Delta\varphi$) with respect to $(\rho\eta)^{1/2}$ remains valid in the case of the microchannels, despite the fact that the total area has been divided into four subareas. The overlap of the points and the fact that they follow the same trend is a significant issue (trendlines are not shown for simplicity reasons, but the linear equations appear in Fig. 9). It indicates that, although the subareas are located at different sites on the sensor, they are identical in their performance when their compartments are filled with the same viscous liquid. The slopes for all microchannels are the same, and therefore, the sensitivity profile of their subareas is uniform and does not depend on their location on the sensor. In numbers, comparison of the slope values (i.e., sensitivity) among the subareas gives a maximum deviation of 4% and 3% when it is expressed in terms of amplitude and phase, respectively.

Apart from comparison between the microchannels' performance, another interesting feature from Fig. 9 rises through the comparison of the total area sensitivity profile with each of the subareas. Some net values of normalized signal change taken from the total area and one subarea revealed a deviation of approximately 10%, as described before. However, this deviation does not hold for sensitivity and is quite lower, only 1%–5% and 2%–3% for amplitude and phase, respectively. This clearly indicates that confining a sample in a smaller rectangular-shaped subarea of the sensor does not affect the sensitivity profile.

V. Conclusion

In this paper, the separation of a SAW sensor surface into independent subareas was achieved, rendering the former a multisample sensor. For this purpose, PDMS-based microfluidic modules consisting of parallel microchannels were fabricated using soft lithography technique, a fast, versatile, and low-cost procedure; the design limitations and specifications were discussed. The evaluation of the μF-on-SAW setup revealed very interesting points. Comparison of the results deriving from the four subareas showed remarkable uniformity along its compartmentalized subareas, regarding the net values of signal change as well as the sensitivity profiles of those areas; no dependence of the results on the location of the subareas on the sensor was observed, neither on the sequence that the microchannels were used (i.e., $1 \rightarrow 2 \rightarrow 3 \rightarrow 4$ or reverse) proving that the SAW surface compartmentalization is reproducible and reliable.

The design of the module was tailor made in accordance with the size and dimension demands of the specific SAW chip. Despite that, the μF-on-SAW setup appears to be a generic tool that can be incorporated in any available SAW system; in addition, the system exhibits high potentials for biosensing applications such as drug screening or cancer biomarkers, since biomolecule arrays and multisample sensing can be hosted on a single SAW sensor.

Acknowledgment

K. Mitsakakis would like to thank A. Malainou and M. E. Vlachopoulou of the Institute of Microelectronics, National Center for Scientific Research "Demokritos," for assistance in clean room processes and soft lithography, and Dr. F. Bender and Dr. A. Tsortos at the Institute of Molecular Biology and Biotechnology, Foundation for Research and Technology Hellas, for fruitful discussions.

References

[1] S. Kurosawa, T. Hirokawa, K. Kashima, H. Aizawa, D.-S. Han, Y. Yoshimi, Y. Okada, K. Yase, J. Miyake, M. Yoshimoto, and J. Hilborn, "Detection of deposition rate of plasma-polymerized films by quartz crystal microbalance," *Thin Solid Films*, vol. 374, no. 2, pp. 262–267, Oct. 2000.

[2] C.-Y. Shen, C.-P. Huang, and W.-T. Huang, "Gas-detecting properties of surface acoustic wave ammonia sensors," *Sens. Actuators B, Chem.*, vol. 101, no. 1/2, pp. 1–7, Jun. 2004.

[3] A. Tsortos, G. Papadakis, K. Mitsakakis, K. A. Melzak, and E. Gizeli, "Quantitative determination of size and shape of surface-bound DNA using an acoustic wave sensor," *Biophys. J.*, vol. 94, no. 7, pp. 2706–2715, Apr. 2008.

[4] T. M. A. Gronewold, "Surface acoustic wave sensors in the bioanalytical field: Recent trends and challenges," *Anal. Chim. Acta*, vol. 603, no. 2, pp. 119–128, Nov. 2007.

[5] M. Jungwirth, H. Scherr, and R. Weigel, "Micromechanical precision pressure sensor incorporating SAW delay lines," *Acta Mech.*, vol. 158, no. 3/4, pp. 227–252, Sep. 2002.

[6] A. J. Ricco and S. J. Martin, "Acoustic wave viscosity sensor," *Appl. Phys. Lett.*, vol. 50, no. 21, pp. 1474–1476, May 1987.

[7] J. Hossenlopp, L. Jiang, R. Cernosek, and F. Josse, "Characterization of epoxy resin (SU-8) film using thickness-shear mode (TSM) resonator under various conditions," *J. Polym. Sci. B, Polym. Phys.*, vol. 42, no. 12, pp. 2373–2384, Jun. 2004.

[8] K. Länge, B. E. Rapp, and M. Rapp, "Surface acoustic wave biosensors: A review," *Anal. Bioanal. Chem*, vol. 391, no. 5, pp. 1509–1519, Jul. 2008.

[9] M. Rapp, J. Reibel, A. Voigt, M. Balzer, and O. Bülow, "New miniaturized SAW-sensor array for organic gas detection driven by multiplexed oscillators," *Sens. Actuators B, Chem.*, vol. 65, no. 1–3, pp. 169–172, Jun. 2000.

[10] M. Fang, K. Vetelino, M. Rothery, J. Hines, and G. C. Frye, "Detection of organic chemicals by SAW sensor array," *Sens. Actuators B, Chem.*, vol. 56, no. 1/2, pp. 155–157, Jun. 1999.

[11] M. Penza, G. Cassano, and F. Tortorella, "Identification and quantification of individual volatile organic compounds in a binary mixture by SAW multisensor array and pattern recognition analysis," *Meas. Sci. Technol.*, vol. 13, no. 6, pp. 846–858, Jun. 2002.

[12] J. W. Grate, "Acoustic wave microsensor arrays for vapor sensing," *Chem. Rev.*, vol. 100, no. 7, pp. 2627–2647, Jul. 2000.

[13] M. Perpeet, S. Glass, T. Gronewold, A. Kiwitz, A. Malavé, I. Stoyanov, M. Tewes, and E. Quandt, "SAW sensor system for marker-free molecular interaction analysis," *Anal. Lett.*, vol. 39, no. 8, pp. 1747–1757, 2006.

[14] K. Länge, G. Blaess, A. Voigt, R. Götzen, and M. Rapp, "Integration of a surface acoustic wave biosensor in a microfluidic polymer chip," *Biosens. Bioelectron.*, vol. 22, no. 2, pp. 227–232, Aug. 2006.

[15] C. Situma, M. Hashimoto, and S. A. Soper, "Merging microfluidics with microarray-based bioassays," *Biomol. Eng.*, vol. 23, no. 5, pp. 213–231, Oct. 2006.

[16] E. Verpoorte and N. F. de Rooij, "Microfluidics meets MEMS," *Proc. IEEE*, vol. 91, no. 6, pp. 930–953, Apr. 2003.

[17] D. Juncker, H. Schmid, A. Bernard, I. Caelen, B. Michel, N. de Rooij, and E. Delamarche, "Soft and rigid two-level microfluidic networks for patterning surfaces," *J. Micromech. Microeng.*, vol. 11, no. 5, pp. 532–541, Sep. 2001.

[18] E. Delamarche, D. Juncker, and H. Schmid, "Microfluidics for processing surfaces and miniaturizing biological assays," *Adv. Mater.*, vol. 17, no. 24, pp. 2911–2933, Dec. 2005.

[19] G. Sauerbrey, "Verwendung von schwingquarzen zur wägung dünner schichten und zur mikrowägung," *Z. Phys.*, vol. 155, no. 2, pp. 206–222, Apr. 1959.

[20] K. K. Kanazawa and J. G. Gordon, "The oscillation frequency of a quartz resonator in contact with a liquid," *Anal. Chim. Acta*, vol. 175, pp. 99–105, 1985.

[21] S. J. Martin and G. C. Frye, "Surface acoustic wave response to changes in viscoelastic film properties," *Appl. Phys. Lett.*, vol. 57, no. 18, pp. 1867–1869, Oct. 1990.

[22] M. Weiss, W. Welsch, M. von Schickfus, and S. Hunklinger, "Viscoelastic behavior of antibody films on a shear horizontal surface acoustic wave sensor," *Anal. Chem.*, vol. 70, no. 14, pp. 2881–2887, Jul. 1998.

Authorized licensed use limited to: WARWICK UNIVERSITY. Downloaded on January 18, 2010 at 14:32 from IEEE Xplore. Restrictions apply.

[23] H. Wohltjen, "Mechanism of operation and design considerations for surface acoustic wave device vapour sensors," *Sens. Actuators*, vol. 5, no. 4, pp. 307–325, Jul. 1984.
[24] E. Gizeli, "Design considerations for the acoustic waveguide biosensor," *Smart Mater. Struct.*, vol. 6, no. 6, pp. 700–706, Dec. 1997.
[25] T. Nomura, A. Saitoh, and Y. Horikoshi, "Measurement of acoustic properties of liquid using liquid flow SH-SAW sensor system," *Sens. Actuators B, Chem.*, vol. 76, no. 1–3, pp. 69–73, Jun. 2001.
[26] J. Kondoh and S. Shiokawa, "A liquid sensor based on a shear horizontal SAW device," *Electron. Commun. Jpn.*, vol. 76, no. 2, pt. 2, pp. 69–82, 1993.
[27] F. Josse and Z. Shana, "Effects of liquid relaxation time on SH surface waves liquid sensors," *J. Acoust. Soc. Amer.*, vol. 85, no. 4, pp. 1556–1559, Apr. 1989.
[28] J. N. Lee, C. Park, and G. M. Whitesides, "Solvent compatibility of poly(dimethylsiloxane)-based microfluidic devices," *Anal. Chem.*, vol. 75, no. 23, pp. 6544–6554, Dec. 2003.
[29] S. K. Sia and G. M. Whitesides, "Microfluidic devices fabricated in poly(dimethylsiloxane) for biological studies," *Electrophoresis*, vol. 24, no. 21, pp. 3563–3576, Nov. 2003.
[30] J. C. McDonald, D. C. Duffy, J. R. Anderson, D. T. Chiu, H. Wu, O. J. A. Schueller, and G. M. Whitesides, "Fabrication of microfluidic systems in poly(dimethylsiloxane)," *Electrophoresis*, vol. 21, no. 1, pp. 27–40, Jan. 2000.
[31] B.-H. Jo, L. M. van Lerberghe, K. M. Motsegood, and D. J. Beebe, "Three-dimensional micro-channel fabrication in polydimethylsiloxane (PDMS) elastomer," *J. Microelectromech. Syst.*, vol. 9, no. 1, pp. 76–81, Mar. 2000.
[32] M. E. Vlachopoulou, A. Tserepi, N. Vourdas, E. Gogolides, and K. Misiakos, "Patterning of thick polymeric substrates for the fabrication of microfluidic devices," *J. Phys., Conf. Ser.*, vol. 10, pp. 293–296, 2005.

Konstantinos Mitsakakis received the B.Sc. degree in physics from the University of Crete, Heraklion, Greece, in 2003, and the M.Sc. degree in nanosciences and nanotechnologies from the Aristotle University of Thessaloniki, Thessaloniki, Greece, in 2005. He is currently working toward the Ph.D. degree in materials science and technology at the University of Crete, with specialization in biosensors' technology.

He was with the Laboratory for Thin Films-Nanosystems and Nanometrology while at the Aristotle University of Thessaloniki, working on thin-films technology, imaging and nanopatterning of soft materials with scanning probe microscopes. He is currently with the Institute of Molecular Biology and Biotechnology, Foundation for Research and Technology Hellas, Heraklion, and his research interests focus on surface acoustic wave biosensors development and integration with microfluidics.

Angeliki Tserepi received the B.Sc. degree in physics from the National and Kapodistrian University of Athens, Athens, Greece, in 1985, and the M.Sc. and Ph.D. degrees from The Ohio State University, Columbus, in 1990 and 1994, respectively.

She held a Postdoctoral European Fellowship ("Marie Curie") with the University Joseph Fourier of Grenoble, France, during 1994–1996, and with the Institute of Microelectronics (IMEL), National Center for Scientific Research (NCSR) "Demokritos," Greece (Return Grant, Training and Mobility of Researchers), from 1996 to 1997. Since 1997, she has been with IMEL working on plasma processing of materials for applications in micro- and nanotechnology and microsystem fabrication. Her current research interests include fabrication of microfluidic devices and mechanisms for liquid transport in such devices. She is the author or coauthor of six patents and 60 publications in international journals.

Electra Gizeli (M'99) received the B.Sc. degree in chemistry from the National and Kapodistrian University of Athens, Athens, Greece, in 1987, the M.Sc. degree in applied molecular biology and biotechnology from University College London, London, U.K., and the Ph.D. degree in new acoustic wave sensors geometries from the Institute of Biotechnology, University of Cambridge, Cambridge, U.K., in 1993.

Since 2003, she has been a Senior Lecturer with the Department of Biology, University of Crete, Heraklion, Greece, and a Group Leader with the Institute of Molecular Biology and Biotechnology, Foundation for Research and Technology Hellas, Heraklion. Her group's research interests are focused on the study and application of acoustic wave biosensors to biology and biotechnology; more specifically, her work ranges from device fabrication (including single and array-type integrated acoustic wave devices for multisensing analysis) to acoustic wave biosensor application to the study of deoxyribonucleic acid (DNA)–protein interactions and DNA hybridization, investigation of peptide binding to model membranes, and characterization of whole cell-ligand binding assays.

Dr. Gizeli was awarded from the British Biotechnology Science Research Council a Junior David Phillips Research Fellowship and established her group on "Acoustic Biosensors" with the Institute of Biotechnology, University of Cambridge, in 1996. She is a member of the Royal Society of Chemistry, U.K.

Authorized licensed use limited to: WARWICK UNIVERSITY. Downloaded on January 18, 2010 at 14:32 from IEEE Xplore. Restrictions apply.